BIOCHEMISTRY
including biophysical chemistry & molecular biology

Article

pubs.acs.org/biochemistry

Crystal Structure of *Escherichia coli* SsuE: Defining a General Catalytic Cycle for FMN Reductases of the Flavodoxin-like Superfamily

Camden M. Driggers,[†] Paritosh V. Dayal,[‡] Holly R. Ellis,[‡] and P. Andrew Karplus*[,†]

[†]Department of Biochemistry and Biophysics, Oregon State University, 2011 Agricultural and Life Sciences Building, Corvallis, Oregon 97331, United States

[‡]Department of Chemistry and Biochemistry, Auburn University, 179 Chemistry Building, Auburn, Alabama 36849, United States

ABSTRACT: The *Escherichia coli* sulfur starvation utilization (*ssu*) operon includes a two-component monooxygenase system consisting of a nicotinamide adenine dinucleotide phosphate (NADPH)-dependent flavin mononucleotide (FMN) reductase, SsuE, and a monooxygenase, SsuD. SsuE is part of the flavodoxin-like superfamily, and we report here the crystal structures of its apo, FMN-bound, and $FMNH_2$-bound forms at ~2 Å resolution. In the crystals, SsuE forms a tetramer that is a dimer of dimers similar to those seen for homologous FMN reductases, quinone reductases, and the WrbA family of enzymes. A π-helix present at the tetramer building interface is unique to the reductases from two-component monooxygenase systems. Analytical ultracentrifugation studies of SsuE confirm a dimer−tetramer equilibrium exists in solution, with FMN binding favoring the dimer. As the active site includes residues from both subunits, at least a dimeric association is required for the function of SsuE. The structures show that one FMN binds tightly in a deeply held site, which makes available a second binding site, in which either a second FMN or the nicotinamide of NADPH can bind. The $FMNH_2$-bound structure shows subtle changes consistent with its binding being weaker than that of FMN. Combining this information with published kinetic studies, we propose a general catalytic cycle for two-component reductases of the flavodoxin-like superfamily, by which the enzyme can potentially provide $FMNH_2$ to its partner monooxygenase by different routes depending on the FMN concentration and the presence of a partner monooxygenase.

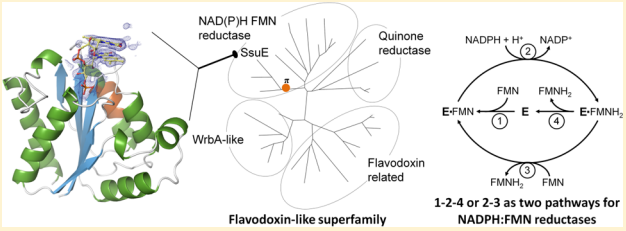

When starved for inorganic sulfur and cysteine, *Escherichia coli* can acquire sulfur from alkanesulfonates through the expression of the proteins of the *ssuEADCB* operon.[1] This operon is transcriptionally induced (reviewed in ref 2) and encodes an ABC-type transporter specific for alkanesulfonates, a nicotinamide adenine dinucleotide phosphate (NADPH)-dependent flavin mononucleotide (FMN) reductase (SsuE), and an $FMNH_2$-dependent alkanesulfonate monooxygenase (SsuD). The latter two enzymes make up a two-component monooxygenase system (Figure 1A) in which SsuE provides $FMNH_2$ to SsuD so it can carry out an oxygen-dependent cleavage of the sulfonate group from compounds such as C-2 to C-10 unsubstituted linear alkanesulfonates, substituted ethanesulfonic acids, and even sulfonated buffers.[3−5]

The sulfur starvation systems of *Pseudomonas putida*[6] and *Pseudomonas aeruginosa*[7] are essentially the same as the *E. coli* SsuE/SsuD system, and species from at least 12 additional genus of bacteria (*Shigella*, *Citrobacter*, *Enterobacter*, *Klebsiella*, *Yokenella*, *Cronobacter*, *Erwinia*, *Pantoea*, *Dickeya*, *Brenneria*, *Serratia*, and *Yersinia*) have a close homologue (>60% sequence identity) to SsuE. For all such species with known genomes, the SsuE gene is clustered with that of an SsuD homologue. In some bacteria, such as *Bacillus subtilis*,[8] *Burkholderia cenocepacia*,[9] and *Corynebacterium glutamicum*,[10] an SsuD homologue is in an operon lacking an SsuE-like reductase. In these organisms, SsuD may not require a specific $FMNH_2$ donor, and cases of flavin reductases associated with a particular two-component system being successfully used in an unrelated system have been reported.[11,12]

Two-component flavin-dependent monooxygenase systems perform a wide variety of reactions,[13] and although the various FMN reductases involved are sometimes mistakenly described as being evolutionarily related (e.g., see Figure 9 of ref 14), those that have been identified actually are of three distinct fold types which, according to the SCOP database, belong to the ferredoxin reductase, the nitroreductase, and the flavodoxin-like superfamilies.

The reductases belonging to the ferredoxin reductase and nitroreductase superfamilies each have a well-defined catalytic cycle characteristic of their superfamily.[13,15] However, for two-component FMN reductases in the flavodoxin-like superfamily, SsuE and EmoB, the reductase component of a two-component system in *Mesorhizobium* sp. BNC1, are the only characterized examples and are reported to have distinct mechanisms.[13,15] For SsuE, as summarized in a recent review,[5] $NADP^+$ inhibition studies[16] together with stopped-flow kinetics[17] and the 1000-fold tighter binding of FMN compared with that of $FMNH_2$ were taken to imply an ordered sequential reaction mechanism in which FMN is not a prosthetic group, but NADPH binds

Received: March 12, 2014
Revised: May 8, 2014
Published: May 9, 2014

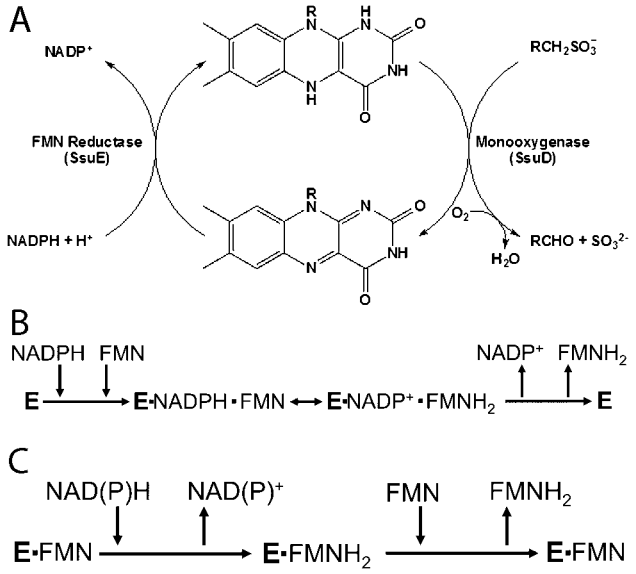

Figure 1. Reactions catalyzed by SsuE and other oxidoreductases of the flavodoxin-like superfamily. (A) Paired reactions catalyzed by the SsuE/SsuD two-component system. (B) Sequential reaction mechanism proposed for SsuE.[13] (C) Ping-pong bisubstrate biproduct reaction mechanism common to EmoB and other NAD(P)H-dependent FMN reductases of the flavodoxin-like superfamily.

first, followed by FMN, which is reduced and then released (Figure 1B). In contrast, for EmoB,[14] kinetic studies and crystal structures have revealed an FMN-bound enzyme that transfers a hydride from NADH to a second FMN in a ping-pong-type reaction mechanism (Figure 1C).

To further investigate the mechanism and properties of *E. coli* SsuE, we have determined crystal structures of the recombinant enzyme with no ligand bound, with FMN bound, and with $FMNH_2$ bound. These structures, together with comparisons with EmoB and other NAD(P)H-dependent FMN reductases in the flavodoxin-like superfamily, lead us to propose a revised mechanism for SsuE that is similar to that of EmoB and the other FMN reductases in this superfamily. We also present a general catalytic cycle that provides a rationale for the differences in the observed kinetics of SsuE and EmoB.

MATERIALS AND METHODS

Protein Purification and Crystallization. Recombinant SsuE was purified as previously described[16] and stored in 25 mM potassium phosphate (pH 7.5), 10% glycerol, and 100 mM NaCl. For crystallization, SsuE was concentrated to ∼10 mg/mL in 10 mM HEPES (pH 7.0). Building on previous work,[18] we grew crystals at room temperature using hanging drops made with 4 μL of a protein stock mixed with 2 μL of a reservoir containing 7.5% (w/v) poly(ethylene glycol) (PEG) 3350 and 0.1 M sodium citrate. For storage and soaks, crystals were transferred to an artificial mother liquor (AML) like the reservoir but with 20% (w/v) PEG 3350. For freezing crystals for data collection, an AML with 20% (w/v) glycerol (and any relevant ligands) was used as a cryoprotectant, and because the crystals were not fully stable in this solution, they were placed in it only briefly (<30 s) before being flash-frozen in liquid nitrogen.

Crystal Soak and Data Collection. For preparing an FMN-bound complex, crystals were soaked in an AML containing 1 mM FMN. Crystals initially showed stress lines

Table 1. Data Collection and Refinement Statistics for SsuE[a]

	apo	FMN-bound	$FMNH_2$-bound
	Data Collection		
unit cell (Å)	$a = b = 185.8$, $c = 91.6$	$a = b = 186.7$, $c = 93.4$	$a = b = 187.0$, $c = 91.3$
resolution (Å)	50−2.10 (2.14−2.10)	50−1.90 (1.93−1.90)	50−2.30 (2.34−2.30)
no. of unique observations	52483 (1922)	75282 (3711)	42033 (2051)
multiplicity	9.5 (3.2)	30.6 (11.7)	19.4 (9.0)
completeness	96.1 (71.1)	100 (100)	100 (98.5)
average I/σ	18.2 (0.36)	46.1 (0.60)	30.7 (0.65)
R_{meas}[b] (%)	0.061 (>0.99)	0.087 (>0.99)	0.10 (>0.99)
R_{pim} (%)	0.021 (>0.99)	0.018 (0.998)	0.026 (0.644)
$CC_{1/2}$[c] (%)	1.00 (0.20)	1.0 (0.32)	1.00 (0.59)
res $\langle I/\sigma \rangle \sim 2$ (Å)[d]	2.4	2.3	2.6
	Refinement		
R_{cryst}/R_{free} (%)	18.0/22.9	17.3/20.8	17.4/22.1
no. of residues	695	694	692
no. of waters	275	380	177
no. of atoms	5781	6124	5758
rmsd for angles (deg)	1.41	1.39	1.39
rmsd for lengths (Å)	0.014	0.012	0.013
φ and ψ favored (%)[e]	96.7	98.1	95.6
φ and ψ outliers (%)[e]	0.15	0	0
$\langle B \rangle$ for protein (Å^2)	61	58	71
$\langle B \rangle$ for FMN1/2 (Å^2)	–	43/77	67
$\langle B \rangle$ for waters (Å^2)	55	56	67
PDB entry	4PTY	4PTZ	4PU0

[a]All crystals belonged to space group $P6_122$. Numbers in parentheses refer to data for the highest-resolution bin. [b]R_{meas} is the multiplicity-weighted merging R factor.[58] [c]$CC_{1/2}$ is the correlation between two data sets each based on half of the data as defined in ref 22. [d]The resolution at which $\langle I/\sigma \rangle \sim 2$ is given to allow comparison with previous standards for selecting high-resolution limits. [e]Ramachandran statistics as defined by Molprobity.[28]

dx.doi.org/10.1021/bi500314f | *Biochemistry* 2014, 53, 3509−3519

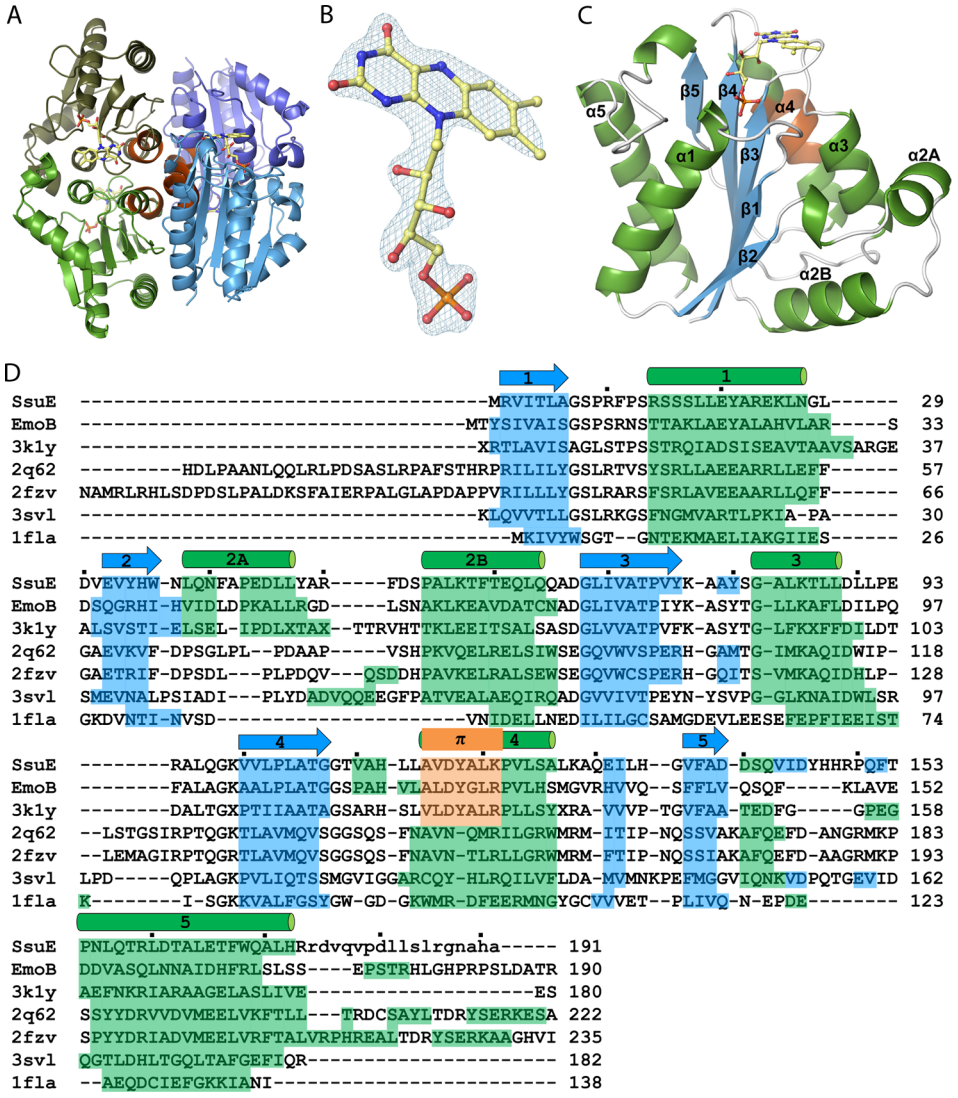

Figure 2. SsuE structure and structure-based sequence alignment with representative homologues. (A) SsuE tetramer made from chains A and B (light green and dark green, respectively) and chains A′ and B′ (light blue and dark blue, respectively) created by the crystallographic 2-fold. Also indicated are the deeply nestled FMN (sticks with yellow carbons) and the π-helix (orange). The half-tetramer formed by chain C (light green) and chain D (light blue) is represented, and the basic dimer is represented by either the green A/B pair or the blue C/D pair. (B) The $2F_o - F_c$ electron density map (contoured at $2.0\rho_{rms}$) for the deeply nestled FMN of chain A calculated after simulated annealing refinement had been conducted with FMN removed from the model (i.e., an annealed omit map). (C) Ribbon drawing of the SsuE monomer with colored and labeled secondary structures (blue for β-strands, green for α-helices, and orange for π-helix). This view is rotated ~90° relative to the light blue chain of panel A. (D) Structure-based sequence alignment with SsuE secondary structure segments annotated and colored as in panel C. Lowercase letters are for residues not built because of uninterpretable density. Shown are the sequences of SsuE, EmoB, an uncharacterized reductase from *Corynebacterium diphtheria* (PDB entry 3k1y), an NADPH-dependent FMN reductase from *Shigella flexneri* (PDB entry 2fzv[52]), the chromate reductase from *E. coli* (PDB entry 3svl[39]), and the G57D mutant flavodoxin from *Clostridium beijerinckii* but with the wild-type sequence shown (PDB entry 1fla[48]).

but were reannealed over ~12 h before being flash-frozen. To obtain an $FMNH_2$ complex, equilibrated FMN-soaked crystals were added to a degassed solution containing 1 mM FMN, 30 mM dithionite, and 50 μM methyl viologen. The blue color of reduced methyl viologen showed that the solution remained reduced during the <10 min soak before the crystals were flash-frozen. $NADP^+$ soaks used $NADP^+$ concentrations from 1 to 100 mM either with or without 5 μM to 1 mM FMN with or without 30 mM dithionite with 50 μM methyl viologen; additional attempts included presoaking crystals in 1 mM FMN and adding varying amounts of either NADPH or $NADP^+$.

Data were collected on beamlines 5.0.1 and 5.0.3 at the Advanced Light Source (Lawrence Berkeley National Laboratory, Berkeley, CA) and using our laboratory Rigaku RU-H3R rotating anode (Cu Kα) and an R-AXIS IV^{++} image plate detector. Synchrotron data sets were processed and scaled using the HKL2000 suite of programs.[19] The R-AXIS IV^{++} data set was processed using imosflm[20] and scaled using Scala[21] from the CCP4 program suite.

Structure Determination and Refinement. Full refinements were initially conducted for each data set using resolution cutoffs based on $\langle I/\sigma \rangle$ values of ≥2 and R_{meas} values of ≤70%. Then, following recommendations showing the value of including weaker data,[22] we reprocessed the data using a $CC_{1/2}$ ~ 0.2 cutoff criterion and extended the resolutions from 2.4 to 2.1 Å for the synchrotron data for apo-SsuE, from 2.3 to 1.9 Å for the data for FMN-bound SsuE, and from 2.6 to 2.3 Å for the data for $FMNH_2$-bound SsuE (Table 1). For all

dx.doi.org/10.1021/bi500314f | *Biochemistry* 2014, 53, 3509−3519

refinements, the same random 5% of data was flagged for use in R_{free} calculations.

Using an initial 2.8 Å resolution laboratory-based data set (data not shown), the crystal structure of apo-SsuE was determined by molecular replacement using Phaser;[23] it placed four copies of a search model comprising chain A of the EmoB structure (PDB entry 4ltd) with all waters removed. Model extension using the AutoBuild option in Phenix[24] led to R and R_{free} values of 33 and 40%, respectively. Further refinements used Coot[25] for manual modeling, Refmac[26] and Buster[27] for minimizations, and Molprobity[28] to monitor the stereochemical quality of the models. TLS refinement was conducted defining each chain as one TLS group. When synchrotron data extending to 2.4 Å resolution became available (Table 1), they were used. During iterative manual model building, 268 water molecules were added in places having $2F_o - F_c$ electron density of $\geq 1\rho_{rms}$, and $F_o - F_c$ density of $\geq 3\rho_{rms}$, that were within 3.7 Å of a potential hydrogen bonding partner. The final model refined using the 2.4 Å high-resolution cutoff had R and R_{free} values of 19.0 and 24.1%, respectively. After the data had been extended to 2.1 Å resolution based on the $CC_{1/2} \sim 0.2$ cutoff criterion,[22] refinement was continued using Phenix. The improved electron density maps allowed further waters to be built and led to lower final R and R_{free} values of 18.0 and 22.9%, respectively, even at the higher 2.1 Å resolution limit (Table 1).

For FMN-bound SsuE, refinement at 2.3 Å resolution began with a partially refined model of apo-SsuE that after rigid-body refinement yielded R and R_{free} values of 27.3 and 32.1%, respectively. Restrained refinement decreased R and R_{free} to 21.3 and 27.7%, respectively, and adding one TLS group per chain produced R and R_{free} values of 19.3 and 24.7%, respectively. Further refinement, including B factor, angle, and distance restraint weight optimization (to 0.3, 1.5, and 3.0, respectively), decreased R and R_{free} to 15.6 and 20.7%, respectively. Once the data had been extended to the $CC_{1/2}$-based 1.9 Å resolution limit, further refinement using Phenix improved the model and expanded it from 226 to 380 waters. The final R and R_{free} values were 17.3 and 20.8%, respectively, at the extended 1.9 Å resolution limit (Table 1), indicating much less overfitting compared to that in the 2.3 Å refinement. Refinement of the $FMHN_2$-bound SsuE also began with a partially refined apo-SsuE model, and using a similar process led to a 2.6 Å resolution model with 144 waters and R and R_{free} values of 18.9 and 23.2%, respectively. Upon resolution extension to the $CC_{1/2}$-based 2.3 Å limit, the number of waters increased to 177 and R and R_{free} decreased to 17.4 and 22.1%, respectively (Table 1). Four, six, and four total side chains were stubbed in the final FMN-bound [0D, 11C, 11A, and 30D (residue number and chain)], $FMNH_2$-bound (0D, 1D, 25C, 44D, 57B, and 97D), and apo structures (0D, 45D, 174B, and 174D), respectively. Also, the default geometry restraints for the FMN forced the entire flavin ring to be in one planar group; before the final rounds of refinement, these were edited to allow for "butterfly" bending by defining two planes in which the N5, N10, and C1′ atoms are in both planar groups.

Spectroscopic Studies of Crystals. UV−vis spectra of crystals prepared identically with the crystals giving the FMN-bound and $FMNH_2$-bound structures were collected at National Synchrotron Light Source beamline X26C. To test for dichroic absorption bands, spectra were recorded for all crystal orientations around a 360° rotation axis with $\kappa = 0$ and using a κ offset of 90° (i.e., a crystal tilt of 45°).

Structure-Based Analyses. Crystal packing interactions were analyzed using PISA.[29] Structural comparisons and structure-based sequence alignments were conducted July 3, 2013, using a Dali search[30] of the Protein Data Bank.[31] For the generation of the phylogenetic tree, all proteins that had a Z score of ≥15 and were ≤90% identical to any other selected protein were selected. Gaps were removed from the SsuE sequence in the Dali alignment, and the format was converted to fasta by Jalview.[32] The phylogenetic tree was generated using Phyml.[33] The names of the families within the flavodoxin-like superfamily are from the SCOP database.[34] For the sequence alignment shown in Figure 2, gaps in the SsuE sequence were not removed.

Analytical Ultracentrifugation. The oligomeric state of SsuE in the absence and presence of flavin was evaluated by sedimentation velocity on an Optima XL-A analytical ultracentrifuge (Beckman Instruments, Palo Alto, CA). Samples of SsuE were exchanged into 25 mM phosphate buffer, 1 mM EDTA, and 0.15 M NaCl (pH 7.0) with an Amicon Ultra-4 instrument with a 10K molecular weight cutoff (Millipore). Three different concentrations of SsuE (12.5, 25, and 37 μM) with and without the addition of an equimolar amount of FMN were loaded into double-sectored cells and equilibrated to 20 °C. Sedimentation data at 280 nm were collected at a rotor speed of 40000 rpm and a radial step size of 0.003 cm. The partial specific volume of 0.7465 cm^3/g was calculated on the basis of the amino acid composition. The buffer density of 1.005235 g/mL was determined using a DA-310 M precision density meter (Mettler Toledo, Hightstown, NJ) at 20 °C. Plots and fits of the data were generated with DCDT+ software using 12−18 consecutive scans for the analysis (version 2.40 from J. S. Philo). Normalized sedimentation coefficient distributions $[g(s^*)]$ were calculated using DCDT+ that utilizes a time derivative approach for sedimentation velocity analysis that includes Lamm equation models of the boundaries.[35,36] The $g(s^*)$ function was fit to a Gaussian curve to determine the concentration, sedimentation coefficients, and diffusion coefficients of a particular species. The curves were best fit to a single-species model.

RESULTS

Overall Structure. Recombinant SsuE crystallized readily in space group $P6_122$ as previously reported,[18] and we determined its structure by molecular replacement using the EmoB crystal structure (37% sequence identity). Structures with reasonable R factors at resolutions near 2 Å (Table 1) were determined in three states: apo-SsuE as grown, an FMN-bound form resulting from a 1 mM FMN soak, and an $FMNH_2$-bound form resulting from dithionite treatment of FMN-soaked crystals. In all of these structures, there are four chains in the asymmetric unit and the protein forms tetramers with 222 symmetry, with chains A and B and chains C and D constituting pairs that make two different kinds of half-tetramers (Figure 2A). In both cases, the full tetramer is created by a crystallographic 2-fold. The packing of the unit cell is such that chains A and C are better fixed in the lattice, having for the FMN-bound structure average B factors of 44 and 48 $Å^2$, respectively, compared with values of 64 and 77 $Å^2$ for chains B and D, respectively. The models for chains A−D include the N-terminal Met (residue 0) through residues 172, 172, 173, and 173, respectively, with reasonably well-defined electron density. The remaining 18 or 19 residues to the C-terminus (residue 191) had no clear electron density and were not modeled. A few side chains without associated

electron density were not modeled beyond Cβ (see Materials and Methods). Unless otherwise specified, descriptions provided are based on chain A but are representative of all the chains.

In describing the overall structure, we will use the FMN-bound form as it is both the highest-resolution structure (1.9 Å) and the one that is most informative about function. As expected, in this complex, all chains have strong $2F_o - F_c$ electron density for one bound FMN (Figure 2B) that is well-ordered and nestled deeply in the protein at the same site that is occupied by FMN in flavodoxins. Also, a second less ordered FMN with interpretable electron density only for the flavin and possibly the phosphate is bound in chains A–C (further discussed below). SsuE has the typical flavodoxin fold with five central parallel β-strands in a β2–β1–β3–β4–β5 arrangement flanked by α-helices, with two helices (α2A and α2B) occurring between β1 and β2 (Figure 2C,D). Another notable secondary structure feature of SsuE is a π-helix,[37] two hydrogen bonds in length, present in helix α4 (Figure 2C,D).

Evolutionary Relationships. In a Dali structural similarity search,[30] all top hits were members of the flavodoxin-like superfamily. The two closest relatives were EmoB (PDB entry 4ltm, 37% sequence identity, 1.6 Å rmsd for 168 C_α atoms)[14] and an uncharacterized oxidoreductase from *Corynebacterium diphtheriae* "3k1y" (PDB entry 3k1y, 29% sequence identity, 2.7 Å rmsd for 160 C_α atoms). In their respective crystals, both of these enzymes form tetramers equivalent to that formed by SsuE (Figure 3A). The 3k1y protein is apparently a reductase in a two-component system as its gene is in a gene cluster encoding an ABC transporter homologue and an SsuD homologue. Including representative more distant relatives found in the Dali search, we created a phylogenetic tree of the flavodoxin-like superfamily (Figure 3B). The tree shows four major groupings, the NAD(P)H:FMN reductases, the quinone reductases, the WrbA-like proteins, and the flavodoxin-related proteins. In this tree, SsuE, EmoB, and the 3k1y protein form a sub-branch of the NADPH:FMN reductase group. We note that the π-helix associated with helix α4 and centered on Tyr118 is found only in the proteins in the SsuE sub-branch and is conserved among them. As is common for π-helices,[37] this is consistent with it being evolutionarily derived by a single-residue insertion that was associated with a gain of function related to the differentiation of the two-component reductase subgroup (see Figure 2D and highlight in Figure 3B).

Although no functionally characterized members of the NADPH:FMN reductase family outside of the SsuE sub-branch are part of a two-component system, all of them catalyze similar chemistry in that they have an FMN prosthetic group that, via a ping-pong-type mechanism like that proposed for EmoB (Figure 1C), can be reduced by NAD(P)H and then reduce a variety of substrates such as quinones, azo dyes, chromate, and cyanide.[38−44] Also, all of them are dimers, tetramers, or proteins having a dimer–tetramer equilibrium, and their geometries of association match the AB dimer and the tetramer of SsuE. As described previously,[44] for tetramer formation there is some variation in the twist between the associating dimer pairs.

Quaternary Structure. The association of the crystal of SsuE into a tetramer that matches the physiologically relevant tetramers of related enzymes (Figure 3B) led us to suspect that it is a physiologically relevant association. This was surprising because we had previously observed that SsuE was a dimer in solution.[1,16] For this reason, we reinvestigated the oligomerization state of SsuE in solution using analytical ultracentrifugation. The data from 12 to 18 consecutive scans were used to obtain the $g^*(s)$ distribution at different SsuE concentrations. The data were best fit to a single-species model as there was no other oligomeric species observed at the concentrations utilized

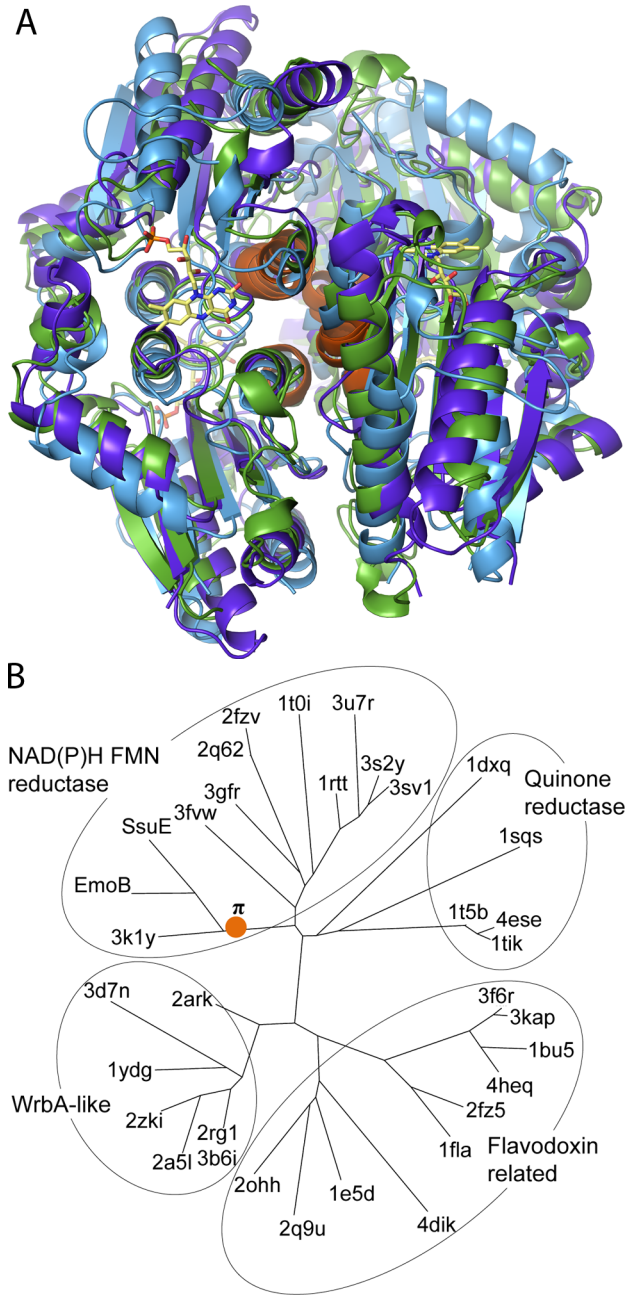

Figure 3. Comparisons of SsuE with its homologues. (A) Overlay of the SsuE (blue), EmoB (green), and 3k1y (purple) tetramers with the deeply nestled FMN from SsuE shown (yellow carbons). The π-helix (orange) is located near the center of the tetramer in all three enzymes. (B) Phylogenic tree of the flavodoxin superfamily including proteins of known structure that aligned with SsuE with a Dali *Z* score of ≥15 and were ≤90% identical to all other hits.[30] The phylogenetic tree was generated using Phyml.[33] The four families making up the flavodoxin-like superfamily are labeled using their SCOP classification.[34] One gene product crystallized without FMN bound by a structural genomics group (PDB entry 3fvw) is unique among the NAD(P)H:FMN reductases in that it does not form a similar dimer or tetramer in the crystal.

dx.doi.org/10.1021/bi500314f | *Biochemistry* 2014, 53, 3509–3519

in the analysis. The SsuE enzyme in the absence of flavin exhibited sedimentation coefficients of 4.6 S to give an average molecular mass of 73.1 ± 6.2 kDa (Figure 4). Given that the monomeric molecular mass of SsuE is 21.3 kDa, the SsuE enzyme exists primarily as a tetramer in the absence of flavin. The SsuE enzyme used in the crystallization trials would predominately exist as a tetramer even before the addition of the crystallization reagents that might promote further association. However, in the presence of 1 equiv of FMN, SsuE gave a sedimentation coefficient of 3.9 S and behaved as a pure dimer with an average molecular mass of 40.9 ± 1.7 kDa (Figure 4).

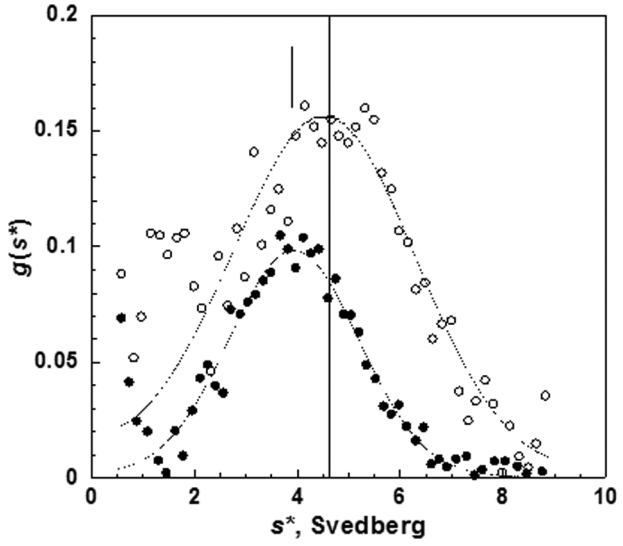

Figure 4. Sedimentation velocity studies of SsuE. Representative $g(s^*)$ distributions based on a single-species model are shown for SsuE (25 μM) in the absence (○) and presence (●) of 25 μM FMN.

The dimer interface between chains A and B buries 1160 Å^2, and the additional surface buried when two dimer pairs come together to form a tetramer is ~2200 Å^2. In contrast, the largest crystal packing interfaces bury ~650 Å^2. Interesting features at the tetramer interface are helix α4 and the π-helix common to SsuE, EmoB, and 3k1y (Figure 3B). This π-helix is located near the center of the tetramer-forming interface (Figure 2A) where the hydroxyl of Tyr118, the conserved residue central to the π-helix, hydrogen bonds across the interface to the O atom of Ala78 in the β3−α3 loop. Because the N atom of Ala78 hydrogen bonds to O4 of the deeply nestled FMN (Figure 5D), this provides a mechanism for how tetramer formation could be influenced by FMN binding. The loop just prior to this helix further links FMN binding with the tetramer interface, as the His112 side chain and the backbone nitrogens of Thr109 and Gly108 hydrogen bond to N3, O2, and N1 of the tightly bound flavin in the same subunit (Figure 5D).

Active Site. When apo-SsuE crystals are soaked in FMN, the *c*-axis increases by ~2% (Table 1), suggesting some conformational changes occur. All chains have a deeply nestled FMN bound in strong density (Figures 2B and 5A), and chains A−C also have a second FMN bound that is highly exposed with its flavin in rather weak electron density (Figure 5A) stacking on top of the flavin of the first FMN. For chain D, in

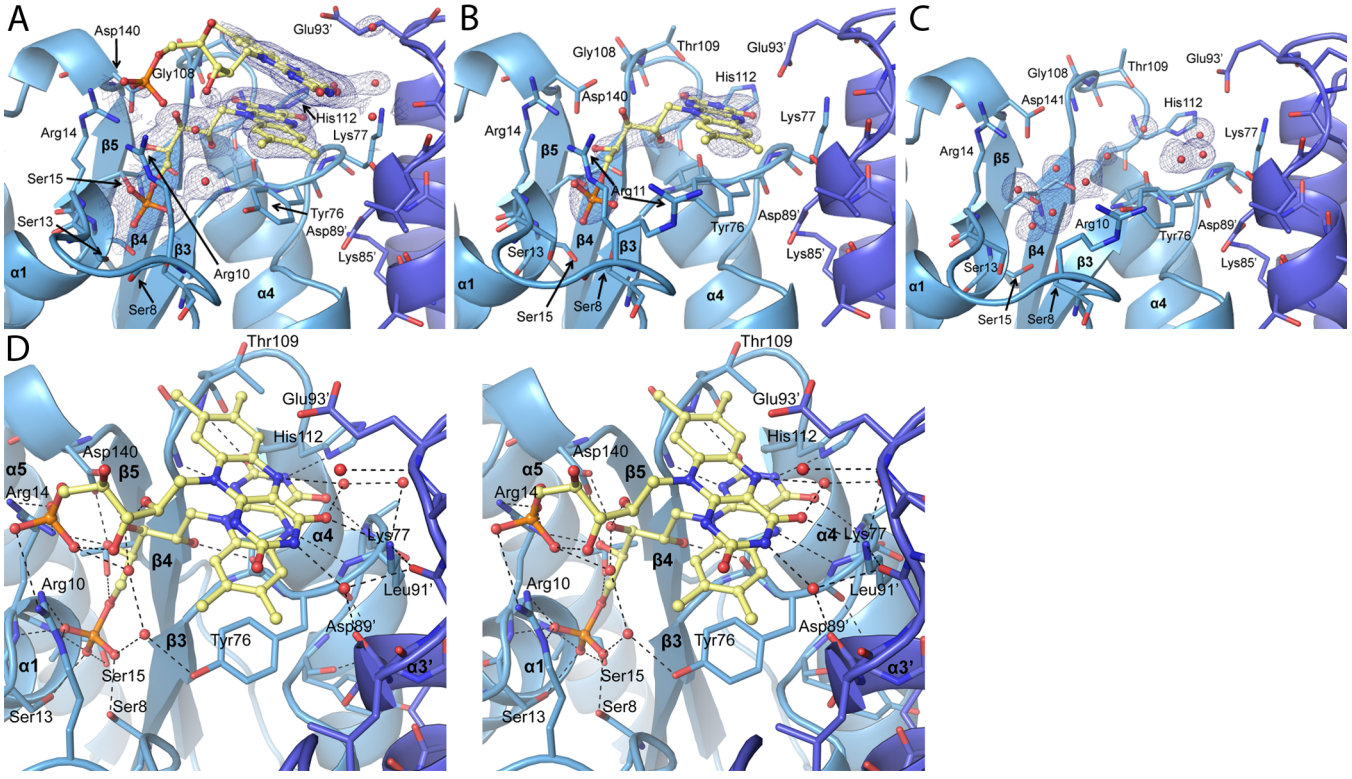

Figure 5. Three forms of the active site of SsuE. (A) FMN-bound SsuE is shown with chain A (light blue) and chain B (dark blue) and $2F_o - F_c$ annealed omit map electron density for the bound FMNs contoured at 1.0ρ_{rms}. (B) $FMNH_2$-bound SsuE shown as in panel A. (C) Apo-SsuE with ordered waters in the active site shown as in panel A. (D) Stereoview of the environment and hydrogen bonding interactions of FMN-bound SsuE. Residues from the dimer mate (chain B) are marked with a prime.

dx.doi.org/10.1021/bi500314f | *Biochemistry* 2014, 53, 3509−3519

which only the first FMN is present, the side chain of His149 from chain B of another tetramer in the crystal rearranges upon FMN binding and stacks above the first flavin blocking the second FMN binding site. This rearrangement of the loop of residues 147−152 in chain B appears to be the main cause of the unit cell change.

The interactions of the well-ordered FMN involve the whole ligand (Figure 5D). The phosphate is coordinated by Ser8, Ser13, Ser15, Arg10, an ordered water molecule that is hydrogen bonded to Tyr76, and the N atom of Arg14. The ribityl is interacting with Thr106, Asp140, Arg14, the O atom of Val75, and an ordered water molecule, and the flavin ring hydrogen bonds with the side chain of His112 (to N3), as well as backbone atoms N of Lys77 (to N5), N of Ala78 (to O4), N of Gly108 (to N1), and N of Thr109 (to O2). Additionally, the binding of the deeply held flavin is influenced by interactions across the dimer interface, with the C7 methyl group just 3.2 Å from the O atom of Asp89′ (the prime indicates a residue from the other subunit of the dimer), with Lys85′ hydrogen bonding to the O atom of Tyr76 and also to the Asp89′ side chain (Figure 5D). The flavin groups are not perfectly planar, having butterfly bends (around the N1−N10 axis) ranging from 3° to 8.5° among the different chains.

The second FMN is rather loosely bound, and the modeled positions of the ribityl and phosphate have very weak electron density reflecting some combination of relatively high disorder and low occupancy (Figure 5A). The only interactions of the putative phosphate and ribityl are with the Arg10 and Arg14 side chains and with the first FMN. The flavin moiety of the second FMN is interacting with the Lys77 amino group (hydrogen bond to O4) and is nicely stacked on the flavin from the first FMN with the N5 atoms just ∼3.5 Å apart. Cross-dimer interactions are fairly extensive, with Glu93′ sitting above the flavin and residues 89′−91′ stabilizing the Lys77 side chain position and a network of waters interacting with flavin atoms N3 and N5 (Figure 5D).

In apo-SsuE, the FMN binding site is occupied by ∼10 ordered waters (Figure 5C). These waters roughly follow the positions to be filled by the FMN ribityl and phosphate groups, with two waters in place of the flavin moiety. The conformational changes associated with FMN binding include small movements of the backbone at residues 9−18, 74−79, 106−111, and 138−158. The largest change is at residues 10−12, where the backbone shifts ∼2 Å and the side chain of Arg10 moves ∼8 Å to an "in" position and becomes much more ordered.

FMN-soaked crystals were treated with dithionite to produce an $FMNH_2$ complex. During this soak, the crystals changed color to pale yellow, indicating a successful reduction of the flavin. In addition, correlated UV−vis spectra of oxidized and reduced SsuE crystals confirmed the presence of the targeted oxidation states (Figure 6). The major change in FMN reduction is that only the deeply seated FMN site is occupied in chains A, C, and D (Figure 5B), and no $FMNH_2$ is bound to chain B. Furthermore, the electron density for the bound $FMNH_2$ molecules is weaker, reflecting either lower occupancy or less rigidity. The lack of $FMNH_2$ binding in chain B may be explained in that Arg10 makes a crystal contact (with Ser141 of chain C′) and this stabilizes the "out" conformation of Arg10 as seen in its temperature factors being lower than those of the other chains. Apparently, the weaker binding of $FMNH_2$ (K_d values of 15.5 and 0.015 μM for $FMNH_2$ and FMN, respectively)[18,45] is not strong enough to cause Arg10 to

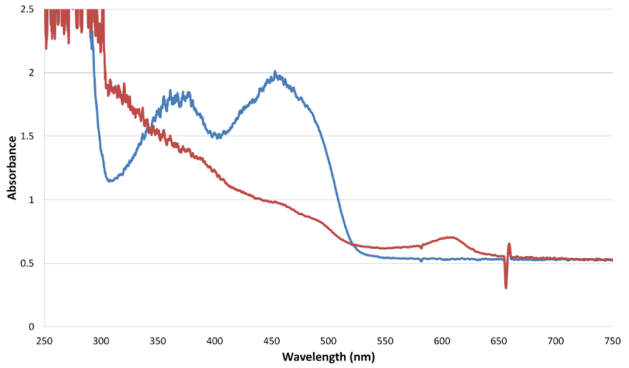

Figure 6. Spectra of SsuE crystals. UV−vis spectra of an FMN-bound (blue) and an $FMNH_2$-bound (red) SsuE crystal before data collection. Multiple crystals soaked under the same condition showed similar spectra. A constant (0.12) was subtracted from all of the values for the red spectrum, so that the two spectra had matching baselines. A small peak at 607 nm not characteristic of $FMNH_2$ can be attributed to reduced methyl viologen present in the soak that produced the reduced crystal.

shift, which happens upon FMN binding. Interestingly, in chains A and C, Arg10 has partial occupancy of the "in" and "out" conformations modeled at 0.67 and 0.33, respectively. On the basis of the assumption that the "in" conformation of Arg10 is tied to FMN binding, we modeled these two $FMNH_2$ ligands at occupancies of 0.67. In chain D, the crystal contact placing His148 above the flavin apparently provides additional stabilization of $FMNH_2$ binding, as it has a higher occupancy (modeled at 1.0 to match the "Arg10-in" conformation of that chain). The butterfly bend of the flavin rings upon treatment with dithionite increases only slightly to range from 6° to 11° among the subunits.

Our attempts to obtain an NADP(H) complex (see Materials and Methods) were not successful. NADP(H) soaks alone resulted in an apo structure, and soaks with FMN and NADP(H) resulted in complexes looking like the FMN complex. A NADP(H) complex was difficult to obtain because the second site is not made available until the first site is occupied, but FMN also competes with NADPH for the second binding site. The shared second binding site provides a structural explanation for the substrate inhibition effect on kinetics observed at high FMN concentrations.[16] Interestingly, a published complex of EmoB with FMN and NADP (PDB entry 2vzj) that was originally interpreted to place the nicotinamide next to the flavin[14] has been reinterpreted to show NADP binding in a nonproductive mode with the adenine stacking on top of the first flavin (PDB entry 4ltn[15]). An overlay of this structure with the dual FMN-bound structures of EmoB and SsuE (Figure 7) shows that the plane of the adenine matches well the positions of the second FMN flavin. The NAD pyrophosphate group and nicotinamide extend in a direction different from that of the ribityl and phosphate of FMN. The only apparent hydrogen bond to this part of the NAD^+ is between the proximal phosphate of NAD and the C3′ ribityl hydroxyl of the first FMN (Figure 7). The minimal interactions with the NMP half of the NAD are consistent with its high temperature factors (∼60 $Å^2$ for the nicotinamide vs ∼30 $Å^2$ for the adenine) and weaker density. No crystal contacts appear to be influencing the NAD binding mode in that crystal.

dx.doi.org/10.1021/bi500314f | *Biochemistry* 2014, 53, 3509−3519

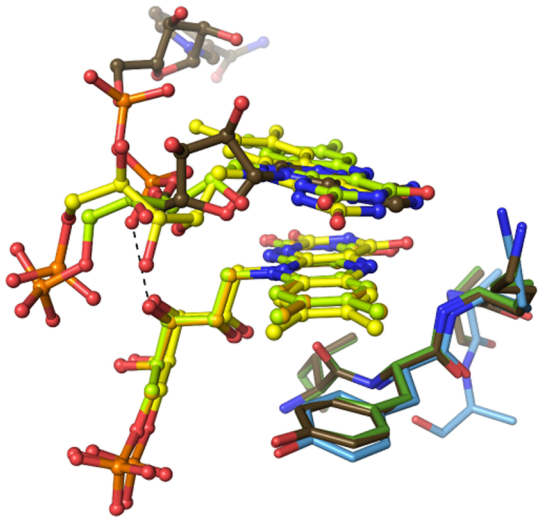

Figure 7. Comparing substrate binding in SsuE and EmoB. Overlay of the active site regions of dual FMN-bound SsuE (yellow carbons for FMN and light blue carbons for protein), dual FMN-bound EmoB (light green carbons for FMN and dark green carbons for protein; PDB entry 4LTM), and the NAD- and FMN-bound EmoB models (orange carbons for FMN and brown carbons for NAD and protein; PDB entry 4LTN). Proteins were aligned using the CEalign feature implemented in Pymol.[57]

DISCUSSION

A prominent theme of these studies of *E. coli* SsuE is that this enzyme has tertiary and quaternary structural properties that are highly similar to those of EmoB and are also quite similar to those of the other reductase branches of the flavodoxin-like superfamily. All members of the flavodoxin-like superfamily bind FMN (or FAD for some quinone reductases) at a common site, which is the deeply nestled first site in SsuE. The flavodoxins themselves are largely monomeric, and for the one flavodoxin known to form a dimer in solution, the dimer is different from that of SsuE and the other flavodoxins.[46] Flavodoxins bind only a single FMN but bind it tightly whether it is in the reduced, semiquinone, or oxidized state. This relates to their function as pure electron transferases that cycle between the oxidized and semiquinone states[47] and is enabled by a conformational change in which the Gly57−Asp58 [numbering for *Clostridium beijernickii* (PDB entry 1fla; Figure 3B)] peptide bond flips upon flavin reduction, allowing the O atom of Gly57 to receive a hydrogen bond from the protonated N5 atom of the semiquinone or hydroquinone flavin, while the N atom of Asp58 donates a hydrogen bond to the lone pair of atom N5 of the oxidized flavin (e.g., ref 48). Also, the flavodoxin flavin is protected from hydride transfer (i.e., two-electron) reactions by having its upper (*si*) surface covered by a Tyr residue.

In contrast, for all of the other branches of the flavodoxin-like superfamily [the WrbA-like proteins, the quinone reductases, and the NAD(P)H-dependent FMN reductases (Figure 3B)], neither the Gly that allows the peptide flip nor the Tyr that covers the *si* face of the flavin is present, making the second site above the flavin available for binding substrates for hydride transfer reactions. All of these enzymes that have been characterized have NAD(P)H:acceptor oxidoreductase activity, where the acceptor may be quinones, FMN, or other assorted substrates.[38,40,44,49−52] Also, for all characterized members of these families except SsuE, the deeply held FMN binds as a prosthetic group and the catalytic cycle proceeds via the ping-pong-type mechanism reported for EmoB (Figure 1C), with the nicotinamide reductant and the FMN, quinone, or other oxidant sequentially occupying the same second binding site.

Interestingly, the basic AB dimer structure seen in SsuE is conserved in all three superfamily branches that are reductases, and in many cases, the tetramer is also conserved. Dimer conservation appears to be related to function because the binding of the nicotinamide, flavin, or quinones in the second site is actually facilitated by the dimer mate. The WrbA-like members all form the same kind of tetramer in their crystals (Figure 3A), and either a tetramer or a dimer−tetramer equilibrium is reported to exist in solution.[49,53,54] In one case, FMN binding is reported to enhance tetramer formation,[54] and in another case, it has no effect.[53] The quinone reductase members are dimers in the crystal, and those that have been characterized are also dimers in solution.[50,51]

The members of the NAD(P)H-dependent FMN reductase family are also dimers or tetramers or are in a dimer−tetramer equilibrium, with one exception being an uncharacterized protein [PDB entry 3fvw (see Results)]. For the enzymes that exist in a dimer−tetramer equilibrium, in some cases tetramer formation is reported to be facilitated by FMN binding[50,51] but in others FMN binding has no effect on quaternary structure.[42,43] SsuE was shown to exist as a tetramer in solution in the absence of flavin and a dimer in the presence of FMN, making it the only known case in which FMN binding weakens tetramer formation. We do not have a good explanation for why earlier gel filtration studies conducted at pH 8 in the absence of flavin showed SsuE to be a dimer.[3] We simply note that the conditions under which the quaternary structure is examined can, of course, influence behavior. For instance, a study at pH 4.0 using ESI-MS showed that the *E. coli* WrbA apoenzyme has a dimer−tetramer equilibrium constant of >30 μM and that FMN concentrations of >25 μM promoted nearly complete tetramer formation.[55] In contrast, studies of the same enzyme using analytical ultracentrifugation at pH 7.9 showed a dimer−tetramer equilibrium constant of 1.4 μM with no change in the presence of FMN.[43]

The fact that FMN weakens the tetramer of SsuE may relate to the unique features of SsuE, EmoB, and 3k1y, which all have the π-helix involving Tyr118 at the tetramer interface. Because the loop preceding it and the π-helix are close to the FMN binding site, it could link FMN binding with tetramer dissociation. As these three enzymes represent a branch of the FMN reductase family that forms an interface with monooxygenases, it may be that the dissociation to dimers facilitates interaction with the partner monooxygenase.

Origins of the Lower Affinity for $FMNH_2$. Another important question relates to the explanation for the affinity for oxidized FMN being 1000-fold higher then that for reduced $FMNH_2$.[16,45] We find the most directly visible contribution for this is tha fact that SsuE does not undergo the peptide flip as seen for flavodoxins. Lys77 is the residue equivalent to the Gly in flavodoxin and is well held in place by hydrogen bonding by backbone and side chains across the dimer interface (Figure 5D). In both oxidized and reduced $FMNH_2$, its backbone amide donates a hydrogen bond to N5 of the oxidized flavin and presumably upon flavin reduction forms an unfavorable electrostatic interaction with the protonated N5 atom. Although other specific interactions that disfavor $FMNH_2$ binding are not visible, the lower occupancy of $FMNH_2$ in

the crystal compared with that of FMN is consistent with it having much weaker binding.

Lys77 is conserved only in the sub-branch that includes EmoB and 3k1y (Figure 3B); however, in every single member of the WrbA-like, quinone reductase-like, and NAD(P)H dependent FMN reductase-like families, the residue is not a Gly, and structural studies suggest that none of these enzymes undergo the peptide flip seen in flavodoxins.

Mechanistic Implications. The high levels of similarity of SsuE to EmoB and the broader reductases in the flavodoxin family make it surprising that SsuE would have a mechanism so distinct from the proposed mechanism (seen in Figure 1B) with NADPH binding first and FMN binding second to make a ternary complex. Furthermore, given the structural features seen here, it is not plausible that NADPH binds before FMN, because the NADPH binding site seen in SsuE (and all of these enzymes) is not present until the first FMN is bound. The question then becomes how our earlier kinetic results supporting the mechanism shown in Figure 1B can be reconciled with this.

In seeking an explanation, we compared the EmoB kinetic work[14] and our kinetic studies of SsuE[16] and discovered that an important difference in these studies is the concentration of FMN under which the studies were conducted. Although our previous inhibition studies were designed to be at "fixed nonsaturating levels of FMN",[16] the studies were conducted at 0.01 μM SsuE and 0.10 μM FMN.[16] These conditions would indeed be nonsaturating for $FMNH_2$ (<1% bound), but given the K_d for FMN, actually ~85% of SsuE would have FMN bound. Taking into consideration the fact that the resting enzyme was not apo but ~85% saturated with FMN, we found the kinetic results showing that NADPH bound "first" would mean that the NADPH was actually binding to the FMN-bound enzyme rather than the apoenzyme. Thus, the binding of FMN prior to NADPH is perfectly consistent with the steady state kinetic data for SsuE.[16] It is also perfectly consistent with our later rapid reaction kinetic studies to determine the rate constants for individual steps in flavin reduction. These studies gave an initial fast phase associated with a charge transfer complex between NADPH and FMN.[17] The rate of this phase showed a hyperbolic dependence on the concentrations of both NADPH and FMN, implying a rapid equilibrium binding of the two substrates. This observed rapid equilibrium binding of NADPH and FMN prior to the generation of the charge transfer complex does not distinguish among pathways involving FMN binding first, NADPH binding first, and a random order of binding. Thus, the data are fully consistent with our structural results that imply that the formation of the FMN-bound SsuE complex allows the binding of NADPH.

This new interpretation, with NADPH associating with the FMN-bound form of the enzyme, is now similar to the behavior of EmoB. The main question remaining is whether the SsuE-bound $FMNH_2$ produced by the transfer of a hydride from NADPH to FMN dissociates from the enzyme or transfers the reducing equivalents to a second "substrate" FMN. In Figure 8, we show a scheme for a general catalytic cycle that allows it to be seen that these two possibilities are simply special cases of a general mechanism that involves four possible steps: (1) FMN binding to the apoenzyme; (2) NADPH binding to the FMN-bound enzyme, transferring a hydride to FMN, and dissociating as $NADP^+$; (3) a second FMN binding, being reduced by the first $FMNH_2$, and dissociation (or being transferred to the partner monooxygenase); and (4) the first $FMNH_2$ dissociating

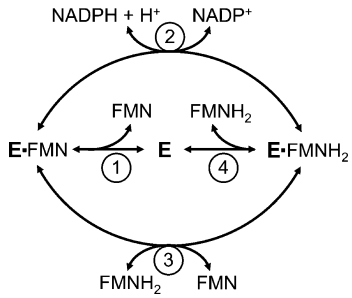

Figure 8. General reaction cycle for the NADPH-dependent FMN reductases in the flavodoxin-like superfamily. When one FMN stays bound and acts as a prosthetic group, once primed by reaction 1, the enzyme cycles repeatedly though steps 2 and 3, and the second FMN acts as a substrate. When the first FMN is weakly bound in its $FMNH_2$ form and/or FMN is at relatively low concentrations, the first $FMNH_2$ may dissociate before an FMN substrate can bind, leading the enzyme to cycle through steps 1, 2, and then 4.

(before a second FMN binds) and re-forming the apoenzyme. The two possible steady state paths around the cycle are 1−2−4 if a single FMN is involved or 2−3 if two FMNs are involved, one as a prosthetic group and the other as a substrate. In the context of this model, the new interpretation is that SsuE follows the 1−2−4 route under conditions like those used in our previous *in vitro* studies[16] (Figure 8). However, in general, the pathway that is followed could vary depending on the affinities of a given enzyme for FMN and $FMNH_2$ as well as their concentrations.

Under the conditions of the EmoB kinetic studies,[14] the enzyme ranges from 54 to 92% saturated with FMN, and we would suggest that some of the enzyme follows the 1−2−4 route while most of the enzyme follows the 2−3 route. Such a mixture of paths could explain the relatively poor fit seen at low FMN concentrations (see Figure 6A of ref 14) when the data are fit to the strictly 2−3 mechanistic model. We suggest that *in vitro* SsuE and EmoB can proceed though either the 1−2−4 route or the 2−3 route depending on the solution conditions and that the mixture of paths that actually occurs in the bacteria is unknown. It might be even that the enzymes proceed through a different path at different times. Because the total concentration of $FMN(H_2)$ for *E. coli* growing exponentially was ~50 μM,[56] it seems that the 2−3 pathway would be taken under these favorable growth conditions where FMN is abundant. However, under the starvation conditions that induce the expression of the SsuE/SsuD system, it is plausible that the enzyme typically proceeds through routes 1, 2, and 4. Furthermore, this scheme also makes it clear how the preferred mechanism could easily be influenced by an association with a partner protein like SsuD.

■ ASSOCIATED CONTENT

Accession Codes

Coordinates and structure factors for the SsuE models have been deposited in the Protein Data Bank as entries 4pty for SsuE in the apo form, 4ptz for SsuE in the oxidized FMN-bound form, and 4pu0 for SsuE in the reduced $FMNH_2$-bound form.

■ AUTHOR INFORMATION

Corresponding Author

*Department of Biochemistry and Biophysics, 2011 Agricultural and Life Sciences Bldg., Oregon State University,

Corvallis, OR 97331. E-mail: karplusp@science.oregonstate.edu. Phone: (541) 737-3200. Fax: (541) 737-0481.

Funding

This project was supported in part by Grant MCB-0545048 to H.R.E. from the National Science Foundation.

Notes

The authors declare no competing financial interest.

■ ACKNOWLEDGMENTS

We thank Drs. Dale Tronrud, Andrea Hall, and Russell Carpenter for useful scientific discussions and help with methods. We also thank Drs. Babak Andi and Allen Orville for collecting coordinated spectroscopic and diffraction data on reduced and oxidized FMN-bound crystals at beamline X26-C at the National Synchrotron Light Source, supported by Contract DE-AC02-05CH11231 from the Office of Basic Energy Sciences of the U.S. Department of Energy. Synchrotron data were collected at the Advanced Light Source, supported by Contract DE-AC02-98CH10886 from the Office of Basic Energy Sciences of the U.S. Department of Energy.

■ ABBREVIATIONS

SsuE and SsuD, sulfur starvation utilization components E and D, respectively; EDTA, ethylenediaminetetraacetic acid; EmoB, EDTA monooxygenase component B; WrbA, tryptophan repressor binding protein; HEPES, 4-(2-hydroxyethyl)-1-piperazineethanesulfonic acid; PEG, poly(ethylene glycol); AML, artificial mother liquor; PDB, Protein Data Bank; ESI-MS, electrospray ionization mass spectrometry; NCS, non-crystallographic symmetry; rmsd, root-mean-square deviation.

■ REFERENCES

(1) van Der Ploeg, J. R., Iwanicka-Nowicka, R., Bykowski, T., Hryniewicz, M. M., and Leisinger, T. (1999) The *Escherichia coli* ssuEADCB gene cluster is required for the utilization of sulfur from aliphatic sulfonates and is regulated by the transcriptional activator Cbl. *J. Biol. Chem. 274*, 29358−29365.

(2) van der Ploeg, J. R., Eichhorn, E., and Leisinger, T. (2001) Sulfonate-sulfur metabolism and its regulation in *Escherichia coli*. *Arch. Microbiol. 176*, 1−8.

(3) Eichhorn, E., van der Ploeg, J. R., and Leisinger, T. (1999) Characterization of a two-component alkanesulfonate monooxygenase from *Escherichia coli*. *J. Biol. Chem. 274*, 26639−26646.

(4) Xiong, J., and Ellis, H. R. (2012) Deletional studies to investigate the functional role of a dynamic loop region of alkanesulfonate monooxygenase. *Biochim. Biophys. Acta 1824*, 898−906.

(5) Ellis, H. R. (2011) Mechanism for sulfur acquisition by the alkanesulfonate monooxygenase system. *Bioorg. Chem. 39*, 178−184.

(6) Kahnert, A., Vermeij, P., Wietek, C., James, P., Leisinger, T., and Kertesz, M. A. (2000) The ssu locus plays a key role in organosulfur metabolism in *Pseudomonas putida* S-313. *J. Bacteriol. 182*, 2869−2878.

(7) Quadroni, M., James, P., Dainese-Hatt, P., and Kertesz, M. A. (1999) Proteome mapping, mass spectrometric sequencing and reverse transcription-PCR for characterization of the sulfate starvation-induced response in *Pseudomonas aeruginosa* PAO1. *Eur. J. Biochem. 266*, 986−996.

(8) van der Ploeg, J. R., Barone, M., and Leisinger, T. (2001) Expression of the *Bacillus subtilis* sulphonate-sulphur utilization genes is regulated at the levels of transcription initiation and termination. *Mol. Microbiol. 39*, 1356−1365.

(9) Iwanicka-Nowicka, R., Zielak, A., Cook, A. M., Thomas, M. S., and Hryniewicz, M. M. (2007) Regulation of sulfur assimilation pathways in *Burkholderia cenocepacia*: Identification of transcription factors CysB and SsuR and their role in control of target genes. *J. Bacteriol. 189*, 1675−1688.

(10) Koch, D. J., Ruckert, C., Rey, D. A., Mix, A., Puhler, A., and Kalinowski, J. (2005) Role of the ssu and seu genes of *Corynebacterium glutamicum* ATCC 13032 in utilization of sulfonates and sulfonate esters as sulfur sources. *Appl. Environ. Microbiol. 71*, 6104−6114.

(11) Louie, T. M., Xie, X. S., and Xun, L. Y. (2003) Coordinated production and utilization of $FADH_2$ by NAD(P)H-flavin oxidoreductase and 4-hydroxyphenylacetate 3-monooxygenase. *Biochemistry 42*, 7509−7517.

(12) Gisi, M. R., and Xun, L. Y. (2003) Characterization of chlorophenol 4-monooxygenase (TftD) and NADH:flavin adenine dinucleotide oxidoreductase (TftC) of *Burkholderia cepacia* AC1100. *J. Bacteriol. 185*, 2786−2792.

(13) Ellis, H. R. (2010) The FMN-dependent two-component monooxygenase systems. *Arch. Biochem. Biophys. 497*, 1−12.

(14) Nissen, M. S., Youn, B., Knowles, B. D., Ballinger, J. W., Jun, S. Y., Belchik, S. M., Xun, L., and Kang, C. (2008) Crystal structures of NADH:FMN oxidoreductase (EmoB) at different stages of catalysis. *J. Biol. Chem. 283*, 28710−28720.

(15) Driggers, C. M., Ellis, H. R., and Karplus, P. A. (2012) Crystal Structure of *Escherichia coli* NADPH FMN reductase SsuE with and without bound FMN. *Proceedings of the 17th International Symposium of Flavins and Flavoproteins 17*, 613−618.

(16) Gao, B., and Ellis, H. R. (2005) Altered mechanism of the alkanesulfonate FMN reductase with the monooxygenase enzyme. *Biochem. Biophys. Res. Commun. 331*, 1137−1145.

(17) Gao, B., and Ellis, H. R. (2007) Mechanism of flavin reduction in the alkanesulfonate monooxygenase system. *Biochim. Biophys. Acta 1774*, 359−367.

(18) Gao, B., Bertrand, A., Boles, W. H., Ellis, H. R., and Mallett, T. C. (2005) Crystallization and preliminary X-ray crystallographic studies of the alkanesulfonate FMN reductase from *Escherichia coli*. *Acta Crystallogr. F61*, 837−840.

(19) Otwinowski, Z., and Minor, W. (1997) Processing of X-ray Diffraction Data Collected in Oscillation Mode. *Methods Enzymol. 276*, 307−326.

(20) Leslie, A. (1992) Recent changes to the MOSFLM package for processing film and image plate data. *Joint CCP4+ESF-EAMCB newsletter on protein crystallography*, Vol. *26*, Daresbury Laboratory, Warrington, U.K.

(21) Evans, P. (2006) Scaling and assessment of data quality. *Acta Crystallogr. D62*, 72−82.

(22) Karplus, P. A., and Diederichs, K. (2012) Linking crystallographic model and data quality. *Science 336*, 1030−1033.

(23) McCoy, A. J., Grosse-Kunstleve, R. W., Adams, P. D., Winn, M. D., Storoni, L. C., and Read, R. J. (2007) Phaser crystallographic software. *J. Appl. Crystallogr. 40*, 658−674.

(24) Adams, P. D., Afonine, P. V., Bunkoczi, G., Chen, V. B., Davis, I. W., Echols, N., Headd, J. J., Hung, L. W., Kapral, G. J., Grosse-Kunstleve, R. W., McCoy, A. J., Moriarty, N. W., Oeffner, R., Read, R. J., Richardson, D. C., Richardson, J. S., Terwilliger, T. C., and Zwart, P. H. (2010) PHENIX: A comprehensive Python-based system for macromolecular structure solution. *Acta Crystallogr. D66*, 213−221.

(25) Emsley, P., Lohkamp, B., Scott, W. G., and Cowtan, K. (2010) Features and development of Coot. *Acta Crystallogr. D66*, 486−501.

(26) Murshudov, G. N., Vagin, A. A., and Dodson, E. J. (1997) Refinement of macromolecular structures by the maximum-likelihood method. *Acta Crystallogr. D53*, 240−255.

(27) Bricogne, G. (1993) Direct Phase Determination by Entropy Maximisation and Likelihood Ranking: Status Report and Perspectives. *Acta Crystallogr. D49*, 37−60.

(28) Chen, V. B., Arendall, W. B., III, Headd, J. J., Keedy, D. A., Immormino, R. M., Kapral, G. J., Murray, L. W., Richardson, J. S., and Richardson, D. C. (2010) MolProbity: All-atom structure validation for macromolecular crystallography. *Acta Crystallogr. D66*, 12−21.

(29) Krissinel, E., and Henrick, K. (2007) Inference of macromolecular assemblies from crystalline state. *J. Mol. Biol. 372*, 774−797.

(30) Holm, L., and Rosenstrom, P. (2010) Dali server: Conservation mapping in 3D. *Nucleic Acids Res. 38*, W545−W549.

(31) Berman, H. M., Westbrook, J., Feng, Z., Gilliland, G., Bhat, T. N., Weissig, H., Shindyalov, I. N., and Bourne, P. E. (2000) The Protein Data Bank. *Nucleic Acids Res. 28*, 235−242.
(32) Waterhouse, A. M., Procter, J. B., Martin, D. M., Clamp, M., and Barton, G. J. (2009) Jalview Version 2: A multiple sequence alignment editor and analysis workbench. *Bioinformatics 25*, 1189−1191.
(33) Guindon, S., and Gascuel, O. (2003) A simple, fast, and accurate algorithm to estimate large phylogenies by maximum likelihood. *Syst. Biol. 52*, 696−704.
(34) Murzin, A. G., Brenner, S. E., Hubbard, T., and Chothia, C. (1995) Scop: A Structural Classification of Proteins Database for the Investigation of Sequences and Structures. *J. Mol. Biol. 247*, 536−540.
(35) Stafford, W. F., III (1992) Boundary analysis in sedimentation transport experiments: A procedure for obtaining sedimentation coefficient distributions using the time derivative of the concentration profile. *Anal. Biochem. 203*, 295−301.
(36) Philo, J. S. (2006) Improved methods for fitting sedimentation coefficient distributions derived by time-derivative techniques. *Anal. Biochem. 354*, 238−246.
(37) Cooley, R. B., Arp, D. J., and Karplus, P. A. (2010) Evolutionary origin of a secondary structure: π-Helices as cryptic but widespread insertional variations of α-helices that enhance protein functionality. *J. Mol. Biol. 404*, 232−246.
(38) Gonzalez, C. F., Ackerley, D. F., Park, C. H., and Matin, A. (2003) A soluble flavoprotein contributes to chromate reduction and tolerance by *Pseudomonas putida*. *Acta Biotechnol. 23*, 233−239.
(39) Eswaramoorthy, S., Poulain, S., Hienerwadel, R., Bremond, N., Sylvester, M. D., Zhang, Y. B., Berthomieu, C., Van Der Lelie, D., and Matin, A. (2012) Crystal structure of ChrR: A quinone reductase with the capacity to reduce chromate. *PLoS One 7*, e36017.
(40) Jin, H. J., Zhang, Y. F., Buchko, G. W., Varnum, S. M., Robinson, H., Squier, T. C., and Long, P. E. (2012) Structure Determination and Functional Analysis of a Chromate Reductase from *Gluconacetobacter hansenii*. *PLoS One 7*, e42432.
(41) Agarwal, R., Bonanno, J. B., Burley, S. K., and Swaminathan, S. (2006) Structure determination of an FMN reductase from *Pseudomonas aeruginosa* PA01 using sulfur anomalous signal. *Acta Crystallogr. D62*, 383−391.
(42) Liger, D., Graille, M., Zhou, C. Z., Leulliot, N., Quevillon-Cheruel, S., Blondeau, K., Janin, J., and van Tilbeurgh, H. (2004) Crystal structure and functional characterization of yeast YLR011wp, an enzyme with NAD(P)H-FMN and ferric iron reductase activities. *J. Biol. Chem. 279*, 34890−34897.
(43) Grandori, R., Khalifah, P., Boice, J. A., Fairman, R., Giovanielli, K., and Carey, J. (1998) Biochemical characterization of WrbA, founding member of a new family of multimeric flavodoxin-like proteins. *J. Biol. Chem. 273*, 20960−20966.
(44) Binter, A., Staunig, N., Jelesarov, I., Lohner, K., Palfey, B. A., Deller, S., Gruber, K., and Macheroux, P. (2009) A single intersubunit salt bridge affects oligomerization and catalytic activity in a bacterial quinone reductase. *FEBS J. 276*, 5263−5274.
(45) Zhan, X., Carpenter, R. A., and Ellis, H. R. (2008) Catalytic importance of the substrate binding order for the $FMNH_2$-dependent alkanesulfonate monooxygenase enzyme. *Biochemistry 47*, 2221−2230.
(46) Hsieh, Y. C., Chia, T. S., Fun, H. K., and Chen, C. J. (2013) Crystal Structure of Dimeric Flavodoxin from *Desulfovibrio gigas* Suggests a Potential Binding Region for the Electron-Transferring Partner. *Int. J. Mol. Sci. 14*, 1667−1683.
(47) Sancho, J. (2006) Flavodoxins: Sequence, folding, binding, function and beyond. *Cell. Mol. Life Sci. 63*, 855−864.
(48) Ludwig, M. L., Pattridge, K. A., Metzger, A. L., Dixon, M. M., Eren, M., Feng, Y. C., and Swenson, R. P. (1997) Control of oxidation-reduction potentials in flavodoxin from *Clostridium beijerinckii*: The role of conformation changes. *Biochemistry 36*, 1259−1280.
(49) Andrade, S. L. A., Patridge, E. V., Ferry, J. G., and Einsle, O. (2007) Crystal structure of the NADH:quinone oxidoreductase WrbA from *Escherichia coli*. *J. Bacteriol. 189*, 9101−9107.
(50) Faig, M., Bianchet, M. A., Talalay, P., Chen, S., Winski, S., Ross, D., and Amzel, L. M. (2000) Structures of recombinant human and mouse NAD(P)H:quinone oxidoreductases: Species comparison and structural changes with substrate binding and release. *Proc. Natl. Acad. Sci. U.S.A. 97*, 3177−3182.
(51) Chen, H. Z., Hopper, S. L., and Cerniglia, C. E. (2005) Biochemical and molecular characterization of an azoreductase from *Staphylococcus aureus*, a tetrameric NADPH-dependent flavoprotein. *Microbiology 151*, 1433−1441.
(52) Vorontsov, I. I., Minasov, G., Brunzelle, J. S., Shuvalova, L., Kiryukhina, O., Collart, F. R., and Anderson, W. F. (2007) Crystal structure of an apo form of *Shigella flexneri* ArsH protein with an NADPH-dependent FMN reductase activity. *Protein Sci. 16*, 2483−2490.
(53) Gorman, J., and Shapiro, L. (2005) Crystal structures of the tryptophan repressor binding protein WrbA and complexes with flavin mononucleotide. *Protein Sci. 14*, 3004−3012.
(54) Wolfova, J., Smatanova, I. K., Brynda, J., Mesters, J. R., Lapkouski, M., Kuty, M., Natalello, A., Chatterjee, N., Chern, S. Y., Ebbel, E., Ricci, A., Grandori, R., Ettrich, R., and Carey, J. (2009) Structural organization of WrbA in apo- and holoprotein crystals. *Biochim. Biophys. Acta 1794*, 1288−1298.
(55) Natalello, A., Doglia, S. M., Carey, J., and Grandori, R. (2007) Role of flavin mononucleotide in the thermostability and oligomerization of *Escherichia coli* stress-defense protein WrbA. *Biochemistry 46*, 543−553.
(56) Bennett, B. D., Kimball, E. H., Gao, M., Osterhout, R., Van Dien, S. J., and Rabinowitz, J. D. (2009) Absolute metabolite concentrations and implied enzyme active site occupancy in *Escherichia coli*. *Nat. Chem. Biol. 5*, 593−599.
(57) Shindyalov, I. N., and Bourne, P. E. (1998) Protein structure alignment by incremental combinatorial extension (CE) of the optimal path. *Protein Eng. 11*, 739−747.
(58) Diederichs, K., and Karplus, P. A. (1997) Improved R-factors for diffraction data analysis in macromolecular crystallography. *Nat. Struct. Biol. 4*, 269−275.